Programmable entanglement oscillations in a non Markovian channel

Simone Cialdi,[1,2,*] Davide Brivio,[1] Enrico Tesio,[1] and Matteo G. A. Paris[1]

[1]*Dipartimento di Fisica dell'Università degli Studi di Milano, I-20133 Milano, Italia.*
[2]*INFN, Sezione di Milano, I-20133 Milano, Italia.*
(Dated: September 17, 2010)

We suggest and demonstrate an all-optical experimental setup to observe and engineer entanglement oscillations of a pair of polarization qubits in a non-Markovian channel. We generate entangled photon pairs by spontaneous parametric downconversion (SPDC), and then insert a programmable spatial light modulator in order to impose a polarization dependent phase-shift on the spatial domain of the SPDC output and to create an effective non-Markovian environment. Modulation of the enviroment spectrum is obtained by inserting a spatial grating on the signal arm. In our experiment, programmable oscillations of entanglement are achieved, with the maximally revived state that violates Bell's inequality by 17 standard deviations.

Entanglement of a bipartite system is usually degraded by the interaction of each subsystem with the environment, which induces decoherence, i.e. an irreversibile loss of information from the system to the rest of the universe [1, 2]. If the interaction is Markovian, i.e. the loss of information is unidirectional, from the system to the environment, then entanglement monotonically decreases and may be also destroyed in a finite time [3–6]. On the other hand, when some memory effect is present in the interaction between the system and the environment, i.e. when the noisy channel is non-Markovian [7, 8], then a non monotone behaviour of entanglement and, more generally, of quantum correlations may be observed [9–17]. In fact, entanglement oscillations are expected in continuous variable systems [18, 19], whereas collapses and revivals of entanglement have been observed with polarization qubits [20].

In this Letter we suggest and demonstrate for the first time an experimental setup to observe and engineer entanglement oscillations in a programmable way. We address the spatial domain of spontaneous parametric downconversion, and exploit a programmable spatial light modulator to impose a polarization- and position-dependent phase-shift. Since the polarization qubits are obtained by tracing out the spatial degrees of freedom, our apparatus allow us to analize the entanglement dynamics within the "coherence time" of the effective non-Markovian channel. In this framework an effective environment spectrum is obtained by acting on the spatial profile of the SPDC. In turn, in order to investigate entanglement oscillations we insert a spatial grating on the signal arm to achieve a modulation of the environment spectrum. Besides fundamental interest, our scheme may found applications in engineering decoherence, e.g. in quantum process tomography.

In our setup a two crystal geometry [21–23] is used to produce two-qubit polarization entangled states by type-I downconversion in a non-collinear configuration. The state at the output of the crystal can be written as

$$|\psi\rangle \propto \iint d\theta d\theta' f(\theta,\theta') \left[|H\theta\rangle|H\theta'\rangle + e^{i\Phi(\theta,\theta')}|V\theta\rangle|V\theta'\rangle\right]$$

where $|P\theta\rangle$ denotes a single photon state emitted with polarization $P = H, V$ at angle θ (θ') along the signal (idler) arm, θ and θ' are the shifts from the central emission angle ($\theta_0, \theta'_0 \simeq 3°$), and the integrations range from $-\frac{1}{2}\Delta$ to $\frac{1}{2}\Delta$, Δ being the angular aperture of two slits along the downconversion paths, see Fig. 1.
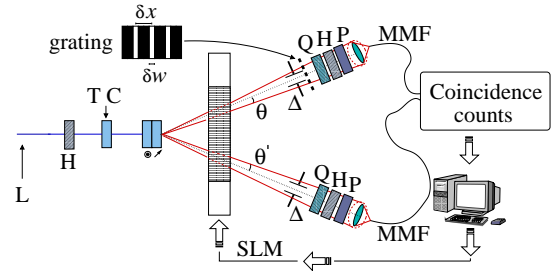

FIG. 1: (Color online) Schematic diagram of experimental setup. A linearly polarized cw laser diode at 406 nm (L) pumps a couple of BBO crystals cut for Type-I downconversion. The horizontal a nd vertical photon pairs are balanced by a half wave-plate set along the pump path, whereas an additional BBO crystal is set on the pump path to compensate the temporal delay. Signal and idler cones travel through the SLM and are spatially selected by two irises and two slits set at $D = 500\,\text{mm}$ with $\Delta x = 5\,\text{mm}$ ($\Delta = 10\,\text{mrad}$). Two long-pass filters cut-on wavelength 715 nm are used to reduce the background. A hand-made grating can be inserted on the signal arm. Photons are focused in two multi-mode fibers (MMF) and sent to single-photon counting modules. Polarizers at the angles 45°, −45° or 45°, 45° are inserted to measure visibility whereas a quarter-wave plate, a half-wave plate and a polarizer are used for the tomographic reconstruction.

The angle-dependent phase-shift $\Phi(\theta,\theta') = \phi(\theta) + \phi'(\theta') + \Phi_0$ comes from the difference between the optical path of vertically polarized photon pair, generated in the first crystal, which must travel along the second

one, and the optical path of the pump beam traversing the first crystal before generating the horizontally polarized pair in the second crystal. These angular dependent terms are responsible for decoherence of polarization qubit and should be removed in order to obtain an effective source of entangled pairs [28]. Upon expanding to first order the terms in $\Phi(\theta, \theta')$ [31], we arrive at $\phi(\theta) = \gamma\theta$ and $\phi'(\theta') = -\gamma\theta'$. In our apparatus, a one dimensional programmable spatial light modulator (SLM), is set both on signal and idler path (see Fig. 1), and is used to achieve a complete purification (i.e., $\Phi = \Phi_0$) by inserting a linear phase function $\phi_{SLM}(\theta) = -\gamma\theta$ on the signal path and $\phi'_{SLM}(\theta') = \gamma\theta'$ on the idler path [29–32]. The constant phase Φ_0 allows to generate different maximally entangled states. In the present experiment we set $\Phi_0 = 0$ by adding a proper constant phase to ϕ_{SLM}. In order to obtain an effective non-Markovian channel the SLM is then used to impose an additional phase function $\phi_s(\theta)$ on the signal arm. Before going to details, let us devote some attention to the angular function $f(\theta, \theta')$, which will be important for the following discussion and assumed to have the factorized form $g(\theta)g'(\theta')$. This assumption has been experimentally verified by measuring the coincidence counts distribution $C = |f_{\exp}(\theta, \theta')|^2$, within a coincidence time window of 50ns, as a function of the signal and idler slit positions θ and θ'. We set two slits of aperture $\Delta x = 1$mm ($\Delta = 2$mrad) along the down-conversion arms and measured coincidence counts within a time window of 10s for slit positions $\theta, \theta' = -2\Delta, -\Delta, \ldots, +2\Delta$. In Fig. 2 we show the experimental data; the phase matching central angles correspond to $\theta, \theta' = 0$. The corresponding coincidence counts distribution has then been compared with the one computed as $\frac{|f_{\exp}(\theta,0)f_{\exp}(0,\theta')|^2}{|f_{\exp}(0,0)|^2}$ and an excellent agreement was found, also corroborated by a significant χ^2 test ($P_{\chi^2 > \chi_0^2} \simeq 0.9$). From the results of Fig. 2 we also infer a Gaussian-like shape for the angular distributions $g(\theta)$, $g'(\theta')$, with a FWHM of 8.6 mrad.
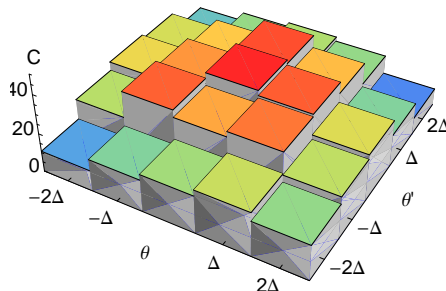

FIG. 2: (Color online) Coincidence counts distribution $C = |f_{\exp}(\theta, \theta')|^2$, within a coincidence time window of 50ns, as a function of the signal and idler slit positions θ and θ'. The phase matching central angles correspond to $\theta, \theta' = 0$.

Once the state has been purified and the addi-

tional phase $\phi_s(\theta) = \alpha\theta$ has been imposed to the signal photon, the dependence on θ' is traced out, and thus no terms containing $g'(\theta')$ appear in the polarization density matrix $\varrho = \text{Tr}_{\theta,\theta'}[|\psi\rangle\langle\psi|] = \frac{1}{2}(|HH\rangle\langle HH| + \varepsilon|VV\rangle\langle HH| + \varepsilon^*|HH\rangle\langle VV| + |VV\rangle\langle VV|)$ where $\varepsilon = \int d\theta\, |g(\theta)|^2\, e^{\imath\alpha\theta}$ is the decoherence factor. It can be shown that, for the state ϱ, the concurrence is $\mathcal{C} = |\varepsilon|$ [20]. Since the angular distribution $g(\theta)$ is symmetric, ε is real and positive, and we may write $\varrho = \varepsilon\varrho_b + (1 - \varepsilon)\varrho_m$, where ϱ_b denotes a Bell state and ϱ_m the corresponding mixture. In turn, in this case, ε equals the interferometric visibility $V(\alpha) = \text{Re}[\varepsilon]$ which, in turn, coincides with the concurrence $\mathcal{C}$. Since we address the spatial domain, it is straightforward to insert an amplitude modulation on $g(\theta)$, e.g. by inserting a physical obstacle along the signal optical path. Moreover, from the expression of the visibility $V(\alpha)$, we see that a periodic structure of the angular distribution would induce oscillations, whereas entanglement decrease and then death may be expected for a non periodic angular distribution. In this framework α may be considered as the evolution parameter of the dynamics of the (noisy) channel. In our apparatus, the amplitude modulation is implemented by means of a hand-made grating with a period δx and a white region width δw centered along the signal arm (see Fig. 1). As we will see, the narrower are the white regions the higher entanglement oscillations are expected. Formally, the insertion of the grating is equivalent to the substitution $g(\theta) \to g(\theta) \cdot m(\theta)$ in the visibility, up to the normalization $\int d\theta\, |g(\theta)m(\theta)|^2 = 1$, where $m(\theta)$ is the periodical unitary step function imposed by the grating. By simply inserting or removing the grating it is possible to compare the different dynamics imposed by a periodical or non-periodical angular distribution.

The experimental setup is shown in Fig. (1): a linearly polarized cw, 406nm laser diode (Thorlabs LPS-406-FC), with a transverse profile TEM_{00}, pumps a couple of 1mm thick BBO crystals cut for Type-I downconversion. The $|HH\rangle$ and $|VV\rangle$ pairs are balanced by a half wave-plate set along the pump path. A BBO crystal with the proper length and optical axis angle is set on the pump path, and is used to counteract the decoherence effect due to the temporal delay between the two components [24–28, 30–32]. This crystal introduce a delay time between the horizontal and vertical polarization of the pump which precompensates the delay time between the $|VV\rangle$ pair generated by the first crystal and the $|HH\rangle$ pair from the second one. Signal and idler cones travel through the SLM and are spatially selected by two irises and two slits set at $D = 500$mm. The low quantum efficiency of our detectors ($\sim 10\%$) forces us to couple large angular regions: we set $\Delta x = 5$mm ($\Delta = 10$ mrad). As we discuss in the following, this will decrease the maximum value of the visibility. The down-conversion output is not

spectrally filtered, whereas two long-pass filters (cut-on wavelength 715nm) are used to reduce the background. A hand-made grating can be inserted on the signal arm. Photons are focused in two multi-mode fibers (MMF) and sent to home-made single-photon counting modules, based on an avalanche photodiode operated in Geiger mode with passive quenching. In order to measure the visibility, we insert two polarizers, set at the angles $45°$, $-45°$ for the minimum and $45°$, $45°$ for the maximum. For the tomographic reconstruction we insert on both paths a quarter-wave plate, a half-wave plate and a polarizer.

After purification we study the behaviour of the visibility as a function of the dimensionless evolution parameter α, governing the linear phase function $\phi_s(\theta) = \alpha\theta$ imposed to the signal by the SLM. As previously discussed, oscillations of entanglement are expected when the grating is inserted. Because of the pixel discretization a step-function with an angular resolution $\zeta = 0.3\,\mathrm{mrad}$ is physically inserted by the SLM in order to approximate the linear functions $\phi_{SLM}(\theta), \phi'_{SLM}(\theta')$. Experimentally, using the SLM, we impose the phase functions

$$\phi^e_{SLM}(n) = -a_{opt}n + b \qquad \text{on idler}$$
$$\phi^e_{SLM}(n) = a_{opt}n + \phi^e_s(n) \qquad \text{on signal},$$

where n is the distance in pixels from the center of the signal beam ($n = 0$ for $\theta = 0$), $a_{opt} = 0.12\,\mathrm{rad/pixel}$ is the optimal slope which allows us to achieve a complete purification, and $b = -\Phi_0$. The linear function $\phi^e_s(n) = a\,n$ is also inserted to study the dynamics, where the experimental evolution parameter is given by $a = \alpha h/L\,\mathrm{rad/pixel}$, $h = 100\mu m$ being the pixel width and $L \simeq 330\mathrm{mm}$ the distance between the SLM and the generating crystals. Since the pixel discretization of the SLM imposes the condition $a \ll 2\pi/\mathrm{pixel}$, high values of a must be neglected in our analysis. We experimentally verified that the curve $V(a)$ saturates to the uncompensated value when $(a+a_{opt}) \to 2\pi$. The revival is expected at $a_{rev} = \frac{2\pi D}{\delta x}\frac{h}{L}$ or, in terms of the angular grating period $\delta\theta$, $\alpha_{rev} = \frac{2\pi}{\delta\theta}$. We choose $\delta x = 2\mathrm{mm}$, which leads at $a_{rev} = 0.476\,\mathrm{rad/pixel}$, in order to avoid high values of the evolution parameter, and we set $\delta w = 0.4\delta x$. In Fig. (3) we present the experimental results, together with the theoretical prediction calculated from the expression of the visibility, as a function of the experimental evolution parameter a. Blue circles and red squares are the experimental data obtained with and without grating, respectively. Blue solid line and red dashed line are the theoretical predictions.

In order to fully characterize the output state we have also performed state reconstruction by polarization qubit tomography for different values of the evolution parameter a. The procedure goes as follows: we measure a suitable set of independent two-qubit projectors [33, 34] and then reconstruct the density matrix from the exper-
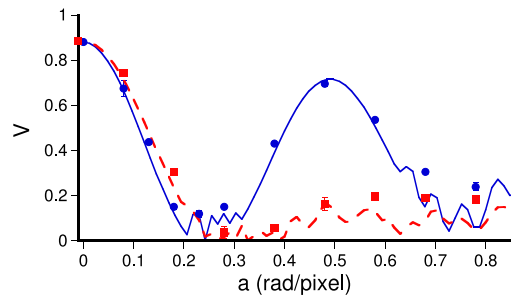

FIG. 3: (Color online) Visibility as a function of the evolution parameter a. Blue circles and red square are the experimental data obtained with and without grating (errors within the symbols). Blue solid line and red dashed line denote the corresponding theoretical predictions.

imental probabilities using maximum-likelihood reconstruction of two-qubit states. The tomographic measurements are obtained by inserting a quarter-wave plate, a half-wave plate and a polarizer. The purification procedure with the grating inserted leads to a visibility $V = 0.881 \pm 0.004$, the density matrix is graphically represented in the upper left panel of Fig. 4. Increasing the evolution parameter to $a = 0.23$, the visibility decreases to $V = 0.120 \pm 0.016$. The corresponding tomographic reconstruction, depicted in the upper right panel of Fig. 4, well illustrate the degradation of entanglement. However, we found an relevant revival after a further increasing of the evolution parameter to $a = 0.48$, where we have $V = 0.696 \pm 0.013$. The corresponding tomographic reconstruction (real and imaginary parts) are reported in the lower panels of Fig. 4. In order to show the revival of the nonlocal correlations we have also measured the Bell parameter $B = |E(\beta_1, \beta_2) + E(\beta_1, \beta'_2) + E(\beta'_1, \beta_2) - E(\beta'_1, \beta'_2)|$ where $E(\beta_1, \beta_2)$ denotes the correlations between measurements performed at polarization angle β_j for the mode j. We found $B = 2.341 \pm 0.019$, which violates CHSH-Bell inequality [35] by more than 17 standard deviations. Comparing this curve with the one obtained without the grating we see that in the latter case no revival occurs after the degradation of entanglement. We also notice that the minimum occurs for lower values of the evolution parameter compared to the case with the grating.

The residual lack of visibility after the purification procedure is mainly due to the very broad downconversion spectral range that is selected by the slits. In fact, with the selected slit aperture, $\Delta x = 5$ mm $\to \Delta = 10\,\mathrm{mrad}$, we estimate that about $200\,\mathrm{nm}$ of the downconversion spectrum are coupled. By narrowing the slit aperture to $\Delta = 4\,\mathrm{mrad}$ only $60\,\mathrm{nm}$ are selected, and the visibility is found to increase at $V = 0.963 \pm 0.005$. This suggests some achromatic effect in the action of the SLM, which prevents a perfect purification. The present experiment
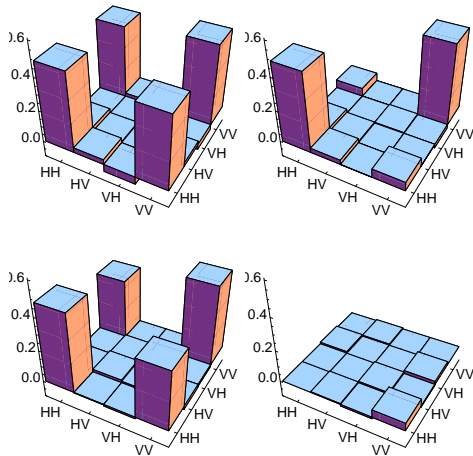
FIG. 4: (Color online) Tomographic reconstruction of a state evolving in the effective non-Markovian channel. In the upper left plot the two-qubit density matrix just after the purification, with visibility $V = 0.881 \pm 0.004$. Upon increasing the evolution parameter to $a = 0.23$ we achieve the minimum of entanglement oscillations: the density matrix is shown in the upper right plot, the corresponding visibility is $V = 0.120 \pm 0.016$. In the lower panels, we show the real and the imaginary part of the reconstructed density matrix at the maximum of entanglement oscillations, which occurs for $a = 0.48$. The corresponding visibility is $V = 0.696 \pm 0.013$, and the Bell parameter $B = 2.341 \pm 0.019$.

has been performed with the larger aperture to compensate the low quantum efficiency of photodetectors.

In conclusion, we have suggested and demonstrated an experimental setup to observe oscillations of polarization entanglement in a programmable way. Our scheme is based on a spatial light modulator, which is inserted on the spatial domain of the downconversion output to achieve an effective non-Markovian environment, and on a grating, which has been employed to create a tunable environment spectrum. Our scheme is all-optical and allows us to generate and detect revivals of entanglement and nonlocality, thus paving the way for engineering of decoherence for polarization qubits.

* Electronic address: simone.cialdi@mi.infn.it
[1] W. H. Zurek, Rev. Mod. Phys. **75**, 715 (2003).
[2] M. Schlosshauer, Rev. Mod. Phys. **76**, 1267 (2005).
[3] T. Yu, J. H. Eberly, Phys. Rev. Lett. **93**, 140404 (2004); Science **323**, 598 (2009).
[4] M. P. Almeida, F. Melo, M. Hor-Meyll, A. Salles, S. P. Walborn, P. H. Souto Ribeiro, and L. Davidovich, Science **316**, 579 (2007).
[5] J. Laurat, K. S. Choi, H. Deng, C. W. Chou, and H. J. Kimble, Phys. Rev. Lett. **99**, 180504 (2007).
[6] J-S. Xu, X-Y. Xu, C-F. Li, C-J. Zhang, X-B. Zou, and G. Guo, Nature Commun. **1**, 1 (2010).
[7] H-P. Breuer, E-M. Laine, J. Piilo, Phys. Rev. Lett. **103**, 210401 (2009).
[8] A. Rivas, S. F. Huelga, M. B. Plenio, Phys. Rev. Lett. **105**, 050403 (2010).
[9] K. Zyczkowski, P. Horodecki, M. Horodecki, R. Horodecki, Phys. Rev A **65**, 012101 (2001).
[10] M. Yonac, J. H. Eberly, Opt. Lett. **33**, 270 (2008).
[11] S. Maniscalco, F. Francica, R. L. Zaffino, N. Lo Gullo, and F. Plastina, Phys. Rev. Lett. **100**, 090503 (2008).
[12] L. Mazzola, S. Maniscalco, J. Piilo, K.-A. Suominen, and B. M. Garraway, Phys. Rev. A **79**, 042302 (2009).
[13] B. Bellomo, R. Lo Franco, S. Maniscalco, and G. Compagno, Phys. Rev. A **78**, 060302(R) (2008).
[14] K. Härkönen, F. Plastina, and S. Maniscalco, Phys. Rev. A **80**, 033841 (2009).
[15] B. Bellomo, R. Lo Franco, and G. Compagno, Phys. Rev. Lett. **99**, 160502 (2007); Adv. Sc. Lett. **2**, 459 (2009).
[16] Q-J. Tong, J-H. An, H-G. Luo, and C. H. Oh, Phys. Rev. A **81**, 052330 (2010).
[17] F. F. Fanchini, T. Werlang, C. A. Brasil, L. G. E. Arruda, A. O. Caldeira, Phys. Rev. A. **81**, 052107 (2010).
[18] S. Maniscalco, S. Olivares, M. G. A. Paris, Phys. Rev. A **75**, 062119 (2007).
[19] R. Vasile, S. Olivares, M. G. A. Paris, S. Maniscalco, Phys. Rev. A **80**, 062324 (2009); R. Vasile, P. Giorda, S. Olivares, M. G. A. Paris, S. Maniscalco, Phys. Rev. A **82**, 012313 (2010).
[20] J.-S. Xu, C-F. Li, M. Gong, X-B. Zou, C-H. Shi, G. Chen, and G-C. Guo, Phys. Rev. Lett. **104**, 100502 (2010).
[21] L. Hardy, Phys. Lett. A **161**, 326 (1992).
[22] P.G. Kwiat, E. Waks, A. G. White, I. Appelbaum, and P.G. Eberhard, Phys. Rev. A **60**, R773 (1999).
[23] M. Genovese, Phys. Rep. **413**, 319 (2005).
[24] Y.-H Kim, S. P. Kulik, Y. Shih, Phys. Rev. A **62**, 011802 (2000).
[25] Y. Nambu, K. Usami, Y. Tsuda, K. Matsumoto, K. Nakamura, Phys. Rev. A **66**, 033816 (2002).
[26] C. Cinelli, G. Di Nepi, F. De Martini, M. Barbieri and P. Mataloni, Phys. Rev. A **70**, 022321 (2004); M. Barbieri, C. Cinelli, F. De Martini and P. Mataloni, Las. Phys. **16**, 1439 (2006).
[27] G. Brida, M. Genovese, M. V. Chekhova, L. A. Krivitsky, Phys. Rev. A **77**, 015805 (2008).
[28] R. Rangarajan, M. Goggin, and P. Kwiat, Opt. Expr. **17**, 18920 (2009).
[29] Z-Q. Zhou, C-F Li, G. Chen, J-S. Tang, Y. Zou, M. Gong, G-C. Guo, Phys. Rev. A. **81**, 064302 (2010).
[30] S. Cialdi, D. Brivio, M. G. A. Paris, Phys. Rev. A **81**, 042322 (2010).
[31] S. Cialdi, D. Brivio, M.G.A. Paris, Appl. Phys. Lett. **97**, 041108 (2010).
[32] S. Cialdi, F. Castelli, I. Boscolo, M. G. A. Paris, Appl. Opt. **47**, 1832 (2008); S. Cialdi, F. Castelli, M. G. A. Paris, J. Mod. Opt. **56**, 215 (2009).
[33] K. Banaszek, G. M. D'Ariano, M. G. A. Paris, M. F. Sacchi, Phys. Rev. A **61** 010304(R) (1999).
[34] D. F. V. James, P. G. Kwiat, W. J. Munro, and A. G. White, Phys. Rev. A **64**, 052312 (2001).
[35] J.F. Clauser, M.A. Horne, A. Shimony, and R.A. Holt, Phys. Rev. Lett. **23**, 880 (1969).